ACS OMEGA

http://pubs.acs.org/journal/acsodf

Article

Efficient Adsorption of Tetracycline from Aqueous Solutions by Modified Alginate Beads after the Removal of Cu(II) Ions

Huayong Luo,* Yu Liu, Hanxing Lu, Qian Fang, and Hongwei Rong*

Cite This: *ACS Omega* 2021, 6, 6240−6251

Read Online

ACCESS | Metrics & More | Article Recommendations | Supporting Information

ABSTRACT: This work dealt with a potential and effective method to reuse modified alginate beads after the removal of Cu(II) ions for efficient adsorption of tetracycline (TC) from aqueous solutions. The modified alginate beads were fabricated by a polyacrylamide (PAM) network interpenetrated in alginate−Ca^{2+} network (PAM/CA) decorated with polyethylene glycol as a pore-forming agent. The porous PAM/CA was characterized using scanning electron microscopy, Brunauer−Emmett−Teller, Fourier transform infrared spectroscopy, and X-ray photoelectron spectroscopy analysis. The adsorption kinetics, isotherms, adsorption stability, and reusability studies of the adsorbent toward Cu(II) ions were scrutinized. The column performance of porous PAM/CA was tested with Cu(II)-containing electroplating wastewater. After Cu(II) adsorption, the Cu(II)-adsorbed PAM/CA (PAM/CA@Cu) was applied to remove TC from aqueous solutions without any regeneration process. The effects of pH, initial TC concentration, ionic strength, and coexisting ions on the adsorption were also discussed in detail. Compared with many reported adsorbents, the PAM/CA@Cu exhibited an excellent adsorption performance toward TC with a maximum adsorption capacity of 356.57 mg/g predicted by the Langmuir model at pH 5.0 and 30 °C with the absence of coexisting ions. The possible adsorption mechanism of TC onto the PAM/CA@Cu was revealed.

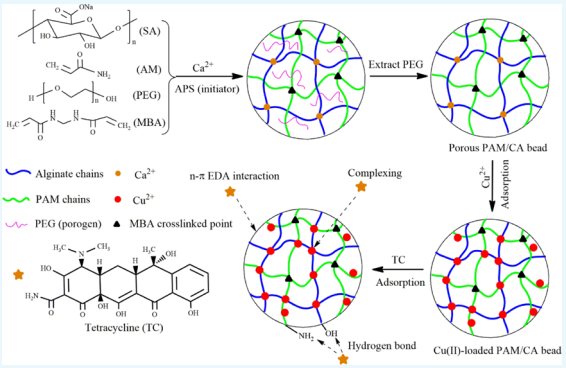

1. INTRODUCTION

Over the recent years, special attention has been paid to Cu(II) ions due to its toxicity.[1,2] A variety of techniques such as chemical precipitation, ion exchange, membrane filtration, solvent extraction, and adsorption have been applied for the removal of heavy-metal ions.[3−5] Among these methods, adsorption has been viewed as one of the most commonly used and effective ways due to its low cost, simplicity, high efficiency, and reversibility.[6−8] Recently, the utilization of natural polymers such as sodium alginate (SA) for the design of biosorbents has been gaining momentum from acknowledging costs and security concerns.[9,10] SA can react with multivalent metal ions such as Ca^{2+} to form a shaped alginate bead, which contributes to its practical application.[11] However, the utilization of alginate bead has been hindered by its disintegration and weak mechanical strength.[9,11,12] To enhance the stability, the fabrication of modified alginate beads by polymer blending to form multicomponent networks provides one of the most versatile and effective ways to develop adsorbents with desirable properties.[13] Polyacrylamide (PAM) is a well-known cheap and easily available synthetic polymer with abundant acyl amino groups, which can act as a functional modifier to achieve higher adsorption amounts of Cu(II) ions.[9] Additionally, polyethylene glycol (PEG) is regarded as a suitable pore-forming agent during the polymerization reaction to make for a porous structure, which would facilitate the diffusion of the adsorbate into the matrix.[11] In these regards, herein, a porous alginate-derived bead constituted of PAM networks interpenetrated in the chains of alginate−Ca^{2+} (PAM/CA) decorated with PEG as a pore-forming agent was developed for the removal of Cu(II) ions.

According to the literature survey, most of adsorbents after the removal of pollutants/metal ions could be used for further capabilities and act as new adsorbents for other contaminations.[6,14,15] Currently, significant concerns have been paid to the presence of antibiotics including tetracycline (TC) in aquatic environments, which is being widely used and may lead to a severe threat to the environment and human health.[16−19] It has been reported that Cu(II) ions could promote the adsorptive removal of TC. Huang et al. found that the presence of Cu(II) in binary systems significantly enhanced the adsorption of TC onto the Fe_3O_4@SiO_2-chitosan/GO (MSCG) nanocomposite, suggesting that Cu(II) ions acted as a bridge between TC and MSCG.[20] Lin's group prepared

Received: November 30, 2020
Accepted: February 19, 2021
Published: March 1, 2021

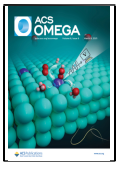

https://dx.doi.org/10.1021/acsomega.0c05807
ACS Omega 2021, 6, 6240−6251

Cu-immobilized alginate beads (SA-Cu) and phenolic hydroxyl (bayberry tannin) functionalized copper alginate (CA-BT) microspheres for effective adsorption of TC, indicating that Cu(II) played an important role in TC adsorption.[21,22] Therefore, the reuse of Cu(II)-adsorbed PAM/CA (PAM/CA@Cu) for TC removal seems to be an economical and potential method. To our knowledge, although several studies have reported the adsorption of Cu(II) ions by alginate-derived adsorbents,[9,23,24] currently there is no report on the reuse of PAM/CA@Cu without any prior treatment for further TC adsorption.

In this paper, we report the fabrication of porous PAM/CA beads for effective removal of Cu(II) ions. The adsorption behaviors of Cu(II) ions onto the porous PAM/CA, including solution pH, kinetics, isotherms, adsorption stability, and reusability, were investigated through batch adsorption and fixed-bed column experiments. Next, the PAM/CA@Cu was used as a new adsorbent for efficient removal of TC, and batch experiments were carried out for solution pH, initial TC concentration, ionic strength, and coexisting ions, kinetics, isotherms, and reusability studies. The possible adsorption mechanisms were revealed through modeling and characterization methods.

2. RESULTS AND DISCUSSION

2.1. Adsorption Studies of Cu(II) Ions. *2.1.1. Effect of pH on Adsorption of Cu(II) Ions.* The effect of pH on the adsorption was examined in the pH range from 2.0 to 6.0 due to the formation of copper hydroxide precipitation at pH greater than 6 (i.e., copper species mainly present as free ionic forms at pH below 6.0).[9] Figure 1 shows that the adsorption

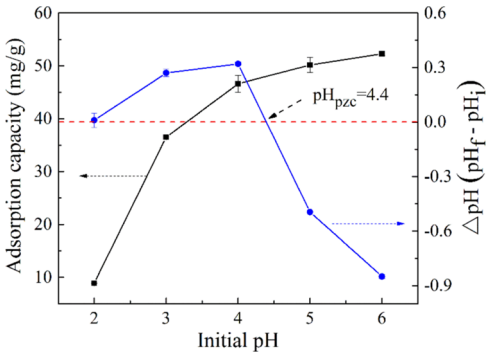

Figure 1. Effect of pH on Cu(II) adsorption and point of zero charge (pH_{pzc}) for the adsorbent.

capacity of Cu(II) ions increased with increasing pH value from its minimum value at pH 2.0 until it reached the maximum value at pH approximately 6.0. This similar situation was reported by others.[9] At a low pH, the competitive effect between H^+ and Cu(II) ions for the active sites of the adsorbent induces poor Cu(II) removal. As the pH value was increased, the aforementioned competition reduced, resulting in a higher adsorption performance. Moreover, the adsorbent surface charge could be partially explicated for the adsorption performances at different pH values. As shown in Figure 1, the pH_{pzc} of porous PAM/CA was close to 4.4, indicating that the adsorbent surface exhibited negative charge and further favored the adsorption of positive charged Cu(II) ions at pH > pH_{pzc}. Thus, the adsorption ability of Cu(II) can be significantly enhanced with increasing pH. To avoid the formation of precipitation, pH 5.0 was chosen and used for the subsequent Cu(II) adsorption experiments.

2.1.2. Adsorption Kinetics and Isotherms of Cu(II) Ions. The curve of adsorption kinetics is shown in Figure 2a. It is clearly found that the adsorption rate of Cu(II) ions was fast at the initial stage, which was followed by a slower adsorption rate until equilibrium. In order to quantitatively evaluate the adsorption kinetics, the experimental data were fitted with the nonlinear pseudo-first-order and pseudo-second-order models. The obtained kinetic parameters are listed in Table S1. The adsorption of Cu(II) ions onto porous PAM/CA could be well described by the pseudo-second-order model, as reflected by the higher correlation coefficient (R^2). The calculated value of q_e (53.18 mg/g) by the pseudo-second-order model was close to the experimental data (50.21 mg/g). Therefore, the adsorption process is mainly controlled by chemisorption.[9]

Figure 2b shows the adsorption isotherms of Cu(II) ions onto porous PAM/CA at 30 °C. The adsorption capacity of Cu(II) ions increased with increasing initial Cu(II) concentration. The experimental data were evaluated by Langmuir and Freundlich models (Figure 2b). The Langmuir model is applicable to homogeneous adsorption, assuming that monolayer adsorption and maximum adsorption occur when adsorbates on the surface of the adsorbent form a saturated layer.[2] The Freundlich isotherm can be used to describe the adsorption on heterogeneous surfaces and multilayer adsorption.[2] The calculated values of the correlation coefficient (Table S1) indicated that both Freundlich and Langmuir models were well fitted with the data for Cu(II) adsorption onto porous PAM/CA (R^2 = 0.933 for the Freundlich model vs R^2 = 0.925 for the Langmuir model). These results agreed with the previous study on the adsorption of Cu(II) onto core−shell poly (vinyl alcohol) (PVA)/SA@PAM beads.[9] Meanwhile, the predicted maximum adsorption capacity for porous PAM/CA (63.45 mg/g) calculated by Langmuir model matched well with the actual adsorption capacity (66.55 mg/g), which was approximately 2 times higher than that of plain calcium alginate beads (34.9 mg/g).[9] These results suggest that the adsorption capacity of porous PAM/CA toward Cu(II) has been improved. Besides, the calculated value of Freundlich adsorption intensity (n) is larger than 1, indicating the favorable condition for adsorption.[25]

2.1.3. Adsorption Stability of Cu(II) Ions onto Porous PAM/CA. For further application of PAM/CA@Cu in the removal of TC, it is required to examine its stability at different pH conditions. Figure 3a shows that Cu(II) ions would be released largely at a lower pH (pH ≤ 2) due to the competitive adsorption of excessive protons for adsorption sites by substituting Cu(II) ions from the surface of the adsorbent, which may be the basis for recovering PAM/CA@Cu for recycling in an acidic solution.[14] Considering that at lower pH (pH = 0.7), the desorption of Cu(II) ions occurred extensively (>99%), the optimal pH value that can be used for Cu(II) ion desorption was fixed at 0.7. However, when the solution pH was higher than 4.0, there was very little leakage of Cu(II) ions due to the chemical bonds involving the chelation of −OH, −COOH, and $-NH_2$ groups of the adsorbent with Cu(II) ions. This phenomenon reveals that PAM/CA@Cu was stable enough and suitable for TC adsorption at a pH higher than 4.0.

2.1.4. Reusability of Porous PAM/CA for Adsorption of Cu(II) Ions. Figure 3b shows the recycling performance of porous PAM/CA for adsorption of Cu(II) ions. The adsorption capacity of Cu(II) exhibited a slight decrease of

https://dx.doi.org/10.1021/acsomega.0c05807
ACS Omega 2021, 6, 6240−6251

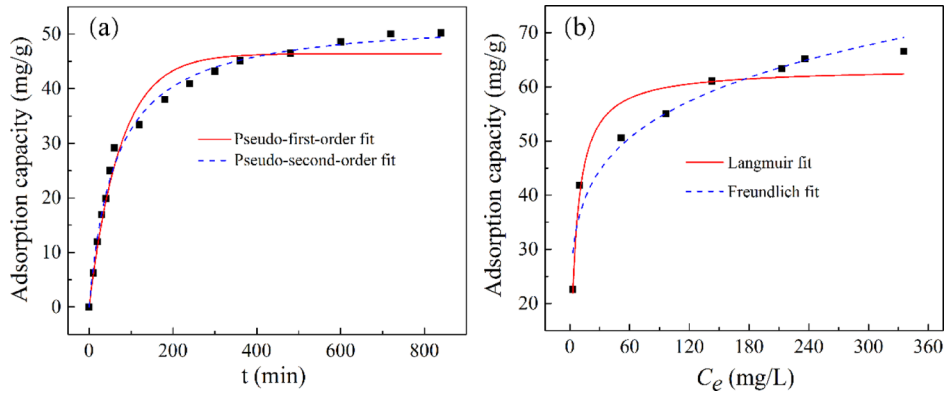

Figure 2. Batch Cu(II) adsorption experiments: (a) kinetics and (b) isotherms.

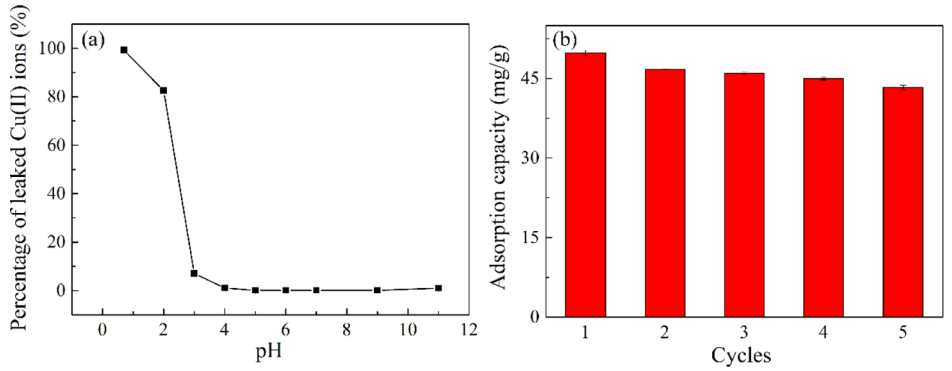

Figure 3. (a) Effect of pH on Cu(II) leakage from PAM/CA@Cu and (b) reusability of porous PAM/CA for adsorption of Cu(II).

13% over five cycles. In addition, the bead adsorbent kept its integrity with nearly unchanged morphology (data not shown). Thus, the porous PAM/CA beads were qualified for practical application due to their high recycling efficiency.

2.1.5. Dynamic Adsorption of Cu(II) Ions in the Fixed-Bed Column. Figure 4 shows the breakthrough curves of Cu(II)

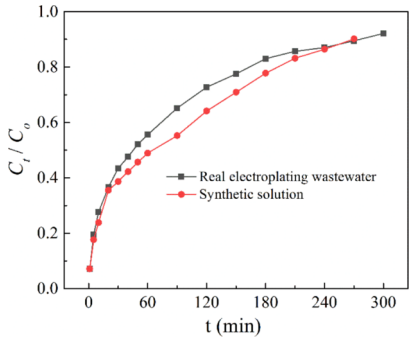

Figure 4. Breakthrough curves for Cu(II) removal from real electroplating wastewater and synthetic solution (adsorbent loading: 2.0 g, bed depth: 18 cm, flow rate: 2.0 mL/min, and influent Cu(II) concentration: 304.4 mg/L).

adsorption onto porous PAM/CA using both synthetic solution and real electroplating wastewater containing Cu(II) ions for comparison under the same pH 2.2. The maximum reaction time and the dynamic adsorption capacity of porous PAM/CA obtained with the sewage were quite similar to those with the synthetic solution. The maximum reaction time for Cu(II) adsorption with both sewage and synthetic solution was around 270 min at a flow rate of 2 mL/min. The dynamic adsorption capacities of porous PAM/CA obtained with sewage and synthetic solution were 25.44 and 28.64 mg/g, respectively (Table 1). These results indicate that the effect of

Table 1. Test Conditions and Results of Cu(II) Column Adsorption

sample	H (cm)	Q (mL/min)	C_o (mg/L)	q_{total} (mg)	q_e (mg/g)
real electroplating wastewater	18	2	304.4	50.89	25.44
synthetic solution	18	2	304.4	57.28	28.64

coexisting ions in the real electroplating wastewater on the continuous adsorption process was almost negligible. Compared with different anions, the influence degree of different cations on Cu(II) adsorption is greater.[26] However, the concentration of Zn^{2+} is very low in the sewage from the experimental section and the other cations (i.e., Na^+ and K^+) exhibit a slight inhibition on the adsorption of Cu(II) due to the lower electric state.[27] As a result, the weak decrease of Cu(II) adsorption capacity could be attributed to the slight inhibition of ionic species contained in the sewage. Overall, the porous PAM/CA beads are capable of removing Cu(II) ions from real electroplating wastewater in the dynamic adsorption system.

2.2. TC Removal Studies. *2.2.1. Effect of pH on TC Removal.* Figure 5a shows the adsorption capacities of TC by porous PAM/CA and PAM/CA@Cu with various initial pHs between 2.0 and 10.0. Obviously, the PAM/CA@Cu showed a higher adsorption capacity toward TC than the PAM/CA. This phenomenon indicated that the immobilization of Cu(II) ions

https://dx.doi.org/10.1021/acsomega.0c05807
ACS Omega 2021, 6, 6240−6251

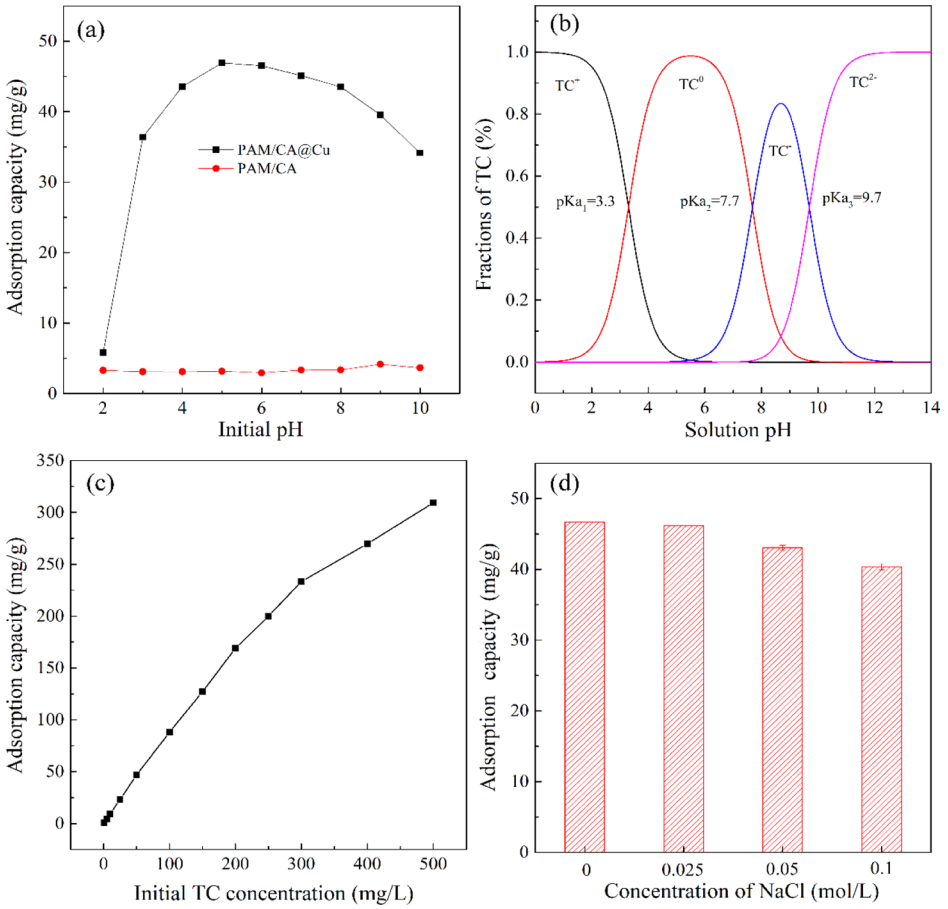

Figure 5. (a) Effect of initial pH on TC removal, (b) distribution of TC species as a function of pH, (c) effect of initial TC concentration on TC removal, and (d) ionic strength on TC removal.

onto the beads played an important role in TC adsorption. Besides, it can be observed that the adsorption process of TC onto PAM/CA@Cu was pH-dependent since pH affected the speciation of TC and surface charge of the adsorbent. As the initial pH value increased, the adsorption capacity of TC initially increased and then decreased after reaching the maximum. The similar trend can be seen in the earlier study.[28] As seen in Figure 5b, TC species dominated by the solution pH were TC^+, TC^0, TC^-, and TC^{2-} when pH < 3.3, 3.3 < pH < 7.7, 7.7 < pH < 9.7, and pH > 9.7, respectively.[18] The pH_{pzc} value of PAM/CA@Cu measured as around 4.5 (Figure S1) denotes that at pH < pH_{pzc} the adsorbent surface is positively charged whereas at pH > pH_{pzc} it is negatively charged. At a lower pH (pH ≤ 2), Cu(II) ions desorbed from PAM/CA@Cu beads. Therefore, the adsorption capacity of TC at pH 2 was low. Although in the pH range of 2−3, a fraction of Cu(II) ions attached on the adsorbent were not leaked out and they were active sites for TC adsorption, the strong electrostatic repulsion between TC species (TC^+) and positively charged surface of the adsorbent inhibited TC adsorption, resulting in low adsorption performance. Conversely, at higher pH (4 < pH < 7), the amounts of Cu(II) ions attached on the adsorbent were not leaked out, which acted as the adsorption sites for TC. Moreover, when the pH was in the range of 4−7, TC molecules became neutral, and the lowest electrostatic repulsion was experienced. Thus, the increase in interaction between TC and PAM/CA@Cu resulted in a higher adsorption capacity of TC. When the pH further increased, the adsorption capacity was decreased. This may be due to the competition for occupying the active sites of the adsorbent by hydroxyl ions with TC. Considering that PAM/CA@Cu achieved the maximum adsorption capacity of TC at pH 5.0, thus other experiments for TC adsorption by the material were conducted at pH 5.0.

2.2.2. Effect of Initial TC Concentration on TC Removal. Figure 5c reveals that the adsorption capacity increased at a higher initial TC concentration. This observation may be due to an elevated adsorbate concentration, which promotes the mass transfer driving force at the solid−liquid interface.[22] The adsorption capacities of PAM/CA@Cu for TC removal were 46. 83−88.18 mg/g with the initial TC concentration range of 50−100 mg/L, which is comparable with that of Cu-immobilized alginate (53.26 mg/g at an initial TC concentration of 90 mg/L),[21] indicating the high efficiency of TC removal by our modified alginate adsorbent.

2.2.3. Effect of Ionic Strength and Coexisting Salts on TC Removal. In order to investigate the adsorption capacity of PAM/CA@Cu toward TC from saline wastewater, the influence of ionic strength on TC adsorption was explored. Figure 5d shows that when the concentration of NaCl increased, the adsorption capacity of TC slightly decreased. At a high concentration of NaCl (0.1 mol/L), PAM/CA@Cu retained 86.5% of its initial adsorption capacity. A similar trend can be observed in the previous study.[21] Moreover, the influences of competing ions by adding other salts (KCl, $NaNO_3$, Na_2SO_4, $MgCl_2$, and $CaCl_2$, respectively) into the

https://dx.doi.org/10.1021/acsomega.0c05807
ACS Omega 2021, 6, 6240−6251

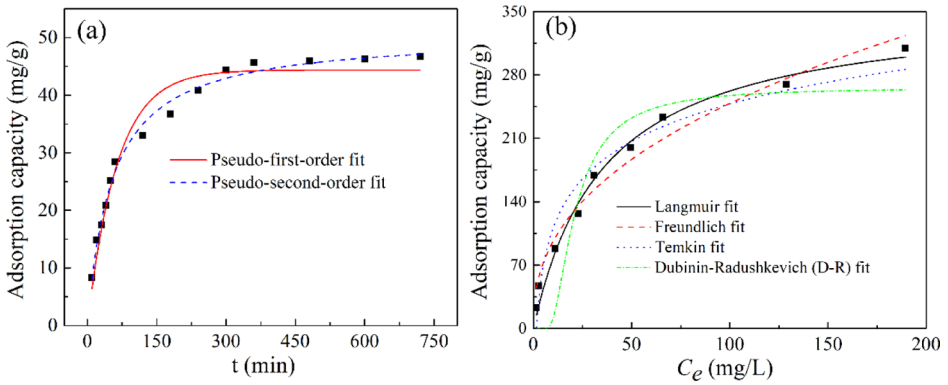

Figure 6. Batch TC adsorption experiments: (a) kinetics and (b) isotherms.

Table 2. Survey of Maximum TC Adsorption Capacities (q_m) (from the Langmuir Model) by Different Adsorbents[a]

adsorbents	conditions	q_m (mg/g)	ref
PAM/CA@Cu beads	pH = 5.0, T = 303 K	356.57	this study
graphene oxide/calcium alginate composite fibers	pH = /, T = 298 K	131.57	17
3D alginate-based MOF hydrogel (MA-M)	pH = 8, T = 298 K	364.89	33
phenolic hydroxyl-derived copper alginate microspheres	pH = 7.0, T = 318.15 K	199.14	22
Cu-immobilized alginate beads	pH = 3.0, T = 318.15 K	58.75	21
Cu and Co nanoparticles codoped MIL-101	pH = 4.8, T = 318 K	161.86	18
carboxymethyl-chitosan-reformed montmorillonite	pH = /, T = 298 K	178.57	34
cerium oxide nanoparticles	pH = /, T = 313 K	57.14	35
alginate/reduced graphene oxide (RGO) double-network hydrogel (GAD)	pH = 8, T = 298 K	290.70	32
alginate/RGO single network hydrogel (GAS)	pH = 8, T = 298 K	247.52	32
alkali–acid-modified magnetic biochar	pH = /, T = 298 K	97.96	28
$MnFe_2O_4$-embedded chitosan-diphenylureaformaldehyde resin	pH = 6, T = /	172.12	36
amino-Fe (III) -functionalized SBA15	pH = 5.0 ± 0.1, T = /	43.07	37
Fe_3O_4@SiO_2-chitosan/graphene oxide nanocomposite	pH = 6.0 ± 0.1, T = 298 K	110.22	20

[a]"/" not available.

adsorption solution were also studied. Figure S2 shows that due to the competition of coexisting ions, all the adsorption capacities exhibited a decreasing trend. The inhibition effect of Na_2SO_4 on TC adsorption was greater than that of KCl and $NaNO_3$. This may be because SO_4^{2-} had more negative charges than Cl^- and NO_3^- at the same concentration, thus causing a stronger competitive adsorption with TC.[18] However, the adsorption capacities decreased significantly due to the existence of $MgCl_2$ and $CaCl_2$ with the concentration of 0.1 mol/L. This may be due to the reaction of Mg^{2+} and Ca^{2+} with the surface functional groups of PAM/CA@Cu and the occupation of adsorption active sites, thus inhibiting the adsorption of TC.[29] Another reason may be that Mg^{2+} and Ca^{2+} could cooperate with TC to form complexes, resulting in the decrease of TC adsorption onto the surface of PAM/CA@Cu.[30]

2.2.4. Adsorption Kinetics and Isotherms of TC. Figure 6a shows that the adsorption of TC rose rapidly during the first 60 min and gradually slowed down until almost reaching the adsorption equilibrium after around 300 min. Compared with the previous study (the adsorption of TC by Cu-immobilized alginate adsorbent reached the equilibrium state at nearly 24 h),[21] TC adsorption in this study requires less time to reach equilibrium. By analyzing the fitting curves (Figure 6a) and calculated kinetics parameters (Table S2), the pseudo-second-order model seems to describe the kinetic data better compared with the pseudo-first-order model, as reflected by the higher correlation coefficient (R^2 = 0.991). This finding indicates that the adsorption of TC onto PAM/CA@Cu is governed by chemisorption.[31]

Figure 6b shows the fitting plots of the experimental data at 30 °C by several isotherm models, and the corresponding parameters are summarized in Table S2. As seen, the Langmuir model can fit the experimental data better in view of its high coefficient (R^2 = 0.987). Moreover, the calculated maximum adsorption capacity (q_m) from the Langmuir model was 356.57 mg/g, which was approximately close to the measured data (309.33 mg/g) at the initial TC concentration of 500 mg/L. These results indicated that the adsorption process of TC could be well described by the Langmuir isotherm model, suggesting that it was a monolayer coverage on a specific homogeneous surface. This finding is similar to the previous studies on the adsorption of TC by alginate-based materials.[22,32] The q_m from the Langmuir model by the present adsorbent was compared with other reported adsorbents listed in Table 2. It was found that the PAM/CA@Cu exhibited much better performance in the removal of TC. Thus, PAM/CA@Cu can be used as a potentially powerful material for TC removal.

2.2.5. Reusability of PAM/CA@Cu for TC Removal. Figure 7 shows that for three cycles, the adsorption capacity of TC onto PAM/CA@Cu remained relatively stable and at a high level as compared with the initial adsorption capacity. This result indicated that the PAM/CA@Cu beads exhibited a favorable reusability and may be a promising candidate for TC removal for practical applications.

https://dx.doi.org/10.1021/acsomega.0c05807
ACS Omega 2021, 6, 6240−6251

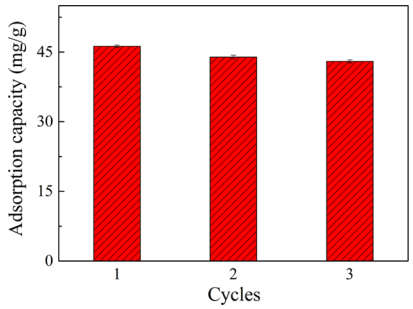

Figure 7. Reusability of PAM/CA@Cu for TC adsorption.

2.3. Characterization Analysis. Figure S3 shows scanning electron microscopy (SEM) images of the porous PAM/CA, PAM/CA@Cu, and PAM/CA@Cu after TC adsorption. From Figure S3a,b, the porous PAM/CA was not a perfect spherical shape with an average diameter of around 2 mm, and its surface was rough and corrugated with many cavities. Similar results can be observed in the previous study.[11] Obviously, the uneven surface and porous structure of the sample would provide the larger contact area between the adsorbate and adsorbent.[21] More importantly, the porous PAM/CA exhibited a bead-like shape, making it easy to achieve separation from the aqueous system and realize the continuous flow fixed-bed column operation. Figure S3c–f shows that the pattern and surface morphology of the adsorbents did not change significantly, indicating that the prepared modified alginate beads remained relatively stable before and after adsorption. Figure S4 shows the nitrogen adsorption–desorption isotherms and pore size distribution curve of porous PAM/CA. It can be seen that the porous PAM/CA yielded a type-IV adsorption–desorption isotherm, evidencing the dominance of mesopores (pore diameters between 2 and 50 nm).[38] The Brunauer–Emmett–Teller (BET) surface area of porous PAM/CA was 28.71 m^2/g. Based on the Barrett–Joyner–Halenda (BJH) method, the total pore volume and average pore diameter of porous PAM/CA were estimated to be 0.04 cm^3/g and 8.66 nm. The BET results together with the SEM images suggested that the prepared modified alginate bead exhibited a porous structure, which could increase the specific surface area and facilitate reactant transport.

Figure 8 presents the Fourier transform infrared (FTIR) spectra of porous PAM/CA, PAM/CA@Cu, and TC-adsorbed PAM/CA@Cu. The peaks for porous PAM/CA (Figure 8a) at 2932, 1090, and 1033 cm^{-1} are associated with saturated C–H groups,[1] –C–O of alcoholic groups,[39] and C–O–C groups,[40] respectively, while those at 1613 and 1419 cm^{-1} may be due to asymmetric and symmetric stretching of the carboxylate group ($-COO^-$).[41] These results suggest the presence of alginate in the hydrogel beads. The enhanced peak at 1667 cm^{-1} represents the carbonyl stretching vibration of the amide bonds.[42] A wide and strong peak at 3418 cm^{-1} from porous PAM/CA (Figure 8a) is the overlay of $-NH_2$ and –OH from PAM and SA, respectively.[43] The various peaks mentioned above could be also detected in both PAM/CA@Cu and TC-adsorbed PAM/CA@Cu, indicating the presence of PAM and SA in the hydrogel beads. After Cu(II) adsorption, the two peaks at 1613 and 1419 cm^{-1} corresponding to the carboxylate group ($-COO^-$) and the peak of $-NH_2$ and –OH at 3418 cm^{-1} shift to different extents (Figure 8b), indicating that the ion exchange between Cu(II) ions and calcium ions was not the main adsorption mechanism but multiple reaction involved

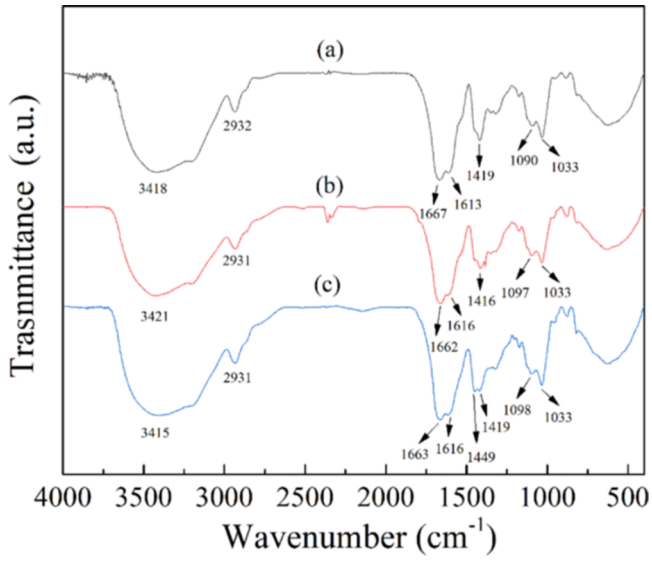

Figure 8. FTIR spectra of (a) porous PAM/CA, (b) PAM/CA@Cu, and (c) PAM/CA@Cu after TC adsorption.

in the Cu(II) adsorption processes, supporting from the introduction of PAM.[9] The characteristic peaks of TC were mainly located in the range of 1700–1200 cm^{-1}, which corresponded to the skeleton vibration absorption peaks of the benzene ring in the TC molecule.[21] After TC adsorption, the characteristic peak at 1449 cm^{-1} (Figure 8c) was assigned to the skeleton vibration of the benzene ring in the TC molecule,[21] confirming that TC molecules were adsorbed onto PAM/CA@Cu. In addition, the peak of $-NH_2$ and –OH at 3421 cm^{-1} is shifted to 3415 cm^{-1} after adsorption of TC (Figure 8c), indicating the intermolecular H-bond with the TC molecule.[31]

2.4. Mechanism Analysis for Cu(II) and TC Adsorption. X-ray photoelectron spectroscopy (XPS) analysis was conducted to understand the interactions between Cu(II) ions and the adsorbent. Figure S5a,b illustrates the fitting curves of C 1s spectra of porous PAM/CA before and after Cu(II) adsorption. The C 1s spectrum of porous PAM/CA can be assigned to peaks at binding energies of 284.80, 285.94, 286.35, and 287.94 eV for the carbon atoms in the C–C, C–N, C–O, and C=O, respectively.[44] However, after Cu(II) adsorption, the binding energies of C–N, C–O, and C=O slightly shifted to higher values of 286.40, 287.89, and 288.75 eV, respectively. These changes indicated the formation of adsorbent–metal complexes, thus reducing the electron density at the adjacent carbon atoms in C–N, C–O, and C=O.[45] From Figure 9a, the O 1s spectrum of porous PAM/CA had three different peaks with binding energies of 533.36 eV (assigned to O–H/C–O–C), 532.44 eV (assigned to O=C–O), and 531.21 eV (assigned to C=O), respectively.[22] After uptake of Cu(II), the binding energies of O atom in O–H/C–O–C, O=C–O, and C=O were all shifted, demonstrating that these groups were involved in the adsorption reaction.[46] Figure 9b shows that the N 1s spectrum of porous PAM/CA comprised two peaks with binding energies of 399.49 eV (assigned to $-NH_2$ from PAM) and 400.87 eV [assigned to O=C–NH– from the methylene bisacrylamide (MBA) unit].[47] The peak of O=C–NH– was weak. The increase in the binding energies after Cu(II) adsorption (Figure 9d) indicated that the surface complexes of R–

https://dx.doi.org/10.1021/acsomega.0c05807
ACS Omega 2021, 6, 6240–6251

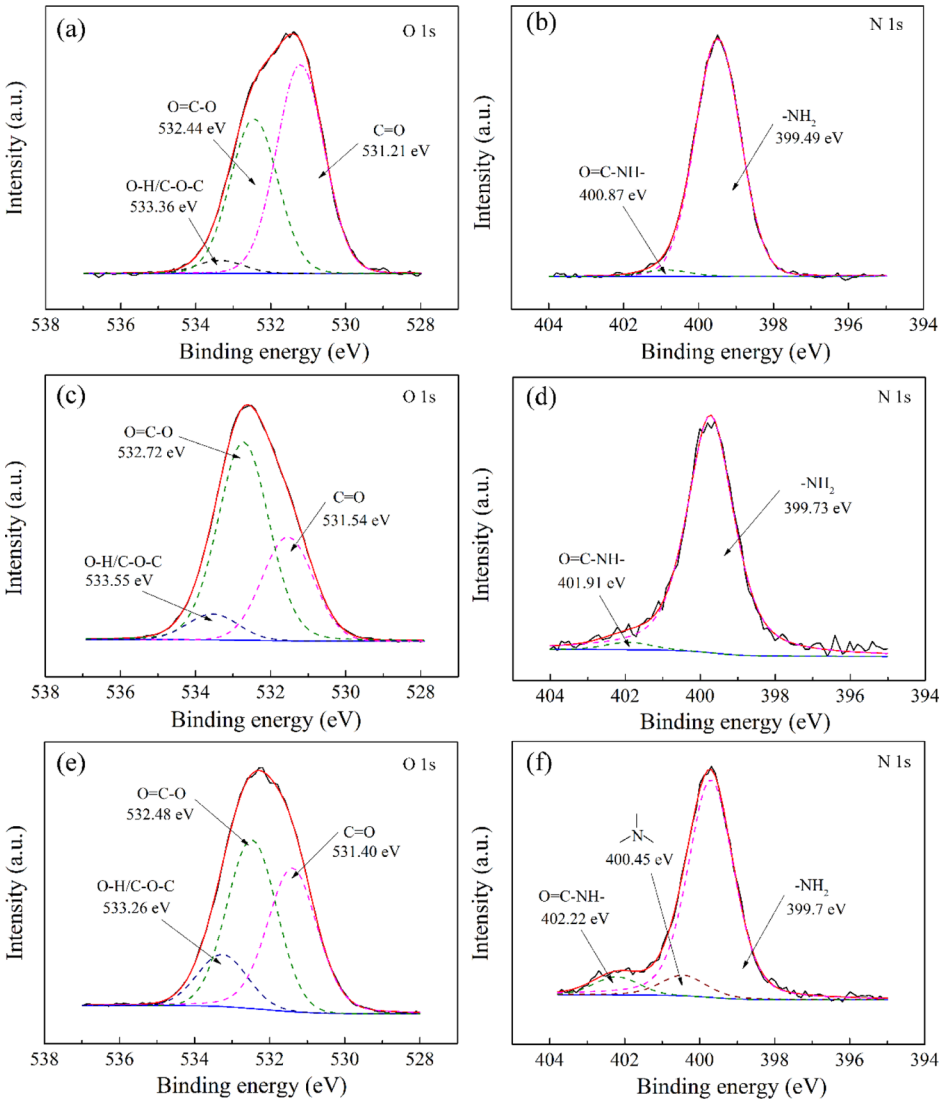

Figure 9. XPS spectra of adsorbents. O 1s of (a) porous PAM/CA, (c) PAM/CA@Cu, and (e) TC-adsorbed PAM/CA@Cu; N 1s of (b) porous PAM/CA, (d) PAM/CA@Cu, and (f) TC-adsorbed PAM/CA@Cu.

NH_2Cu(II) were formed, in which a lone pair of electrons in N atom was donated to the covalent bond between N and Cu(II). Thus, the electron density in N atom was decreased and it consequently led to higher binding energy values.[45] The XPS spectra of Cu 2p in the as-prepared adsorbent after the adsorption of copper ions are shown in Figure S5c. Cu peaks were detected at binding energies of 954.32 eV for Cu(II) $2p_{1/2}$, 952.17 eV for Cu(I) $2p_{1/2}$, 934.78 eV for Cu(II) $2p_{3/2}$, and 932.74 eV for Cu(I) $2p_{3/2}$, respectively. The reduction process might be explained by the existence of large quantities of carbonyl groups and the positive potential of Cu(II).[48] The appearance of satellites demonstrated the presence of Cu^{2+} ions.[47] In general, the mechanism for Cu(II) adsorption onto the porous PAM/CA involved the interactions of N and O atoms with copper. Meanwhile, abundant carbonyl groups also participated in the copper removal, and might reduce Cu(II) to Cu(I).

Based on the experimental results and a review of the literature, the adsorption of TC onto PAM/CA@Cu was a complicated process that might be jointly controlled by both physical and chemical interactions. As confirmed by pH-dependent adsorption analysis, the maximum adsorption capacity of TC was captured at around pH 5.0. At this point, the dominant species of TC is a neutral molecule (TC^0), and only a small amount of TC^+ can be adsorbed by lots of basic sites including −OH groups and N-moieties.[49] As the pH_{pzc} value of PAM/CA@Cu was around 4.5, at the test condition of pH = 5.0 (pH > pH_{pzc}), the negatively charged adsorbent would promote the adsorption of TC^+ through electrostatic interaction. Besides, at around pH 5.0, TC molecules became neutral, which exhibited higher hydrophobic nature between zwitterionic species.[22] Thus, the increment in the adsorption capacity of TC might be contributed by the hydrophobic interaction. Therefore, the physisorption was mainly ascribed to the electrostatic interaction and hydrophobic interaction.

To further illustrate the uptake mechanism, the high-resolution XPS spectra of N 1s, O 1s, and Cu 2p of the adsorbent after TC adsorption were also analyzed. Figure 9f shows that a new peak appeared at 400.45 eV, which was assigned to the tertiary amine structure (−N<).[50] This phenomenon is attributed to the adsorption of TC molecules onto PAM/CA@Cu. Figure 9e shows that after TC adsorption, the binding energies of C═O, O═C−O, and

https://dx.doi.org/10.1021/acsomega.0c05807
ACS Omega 2021, 6, 6240−6251

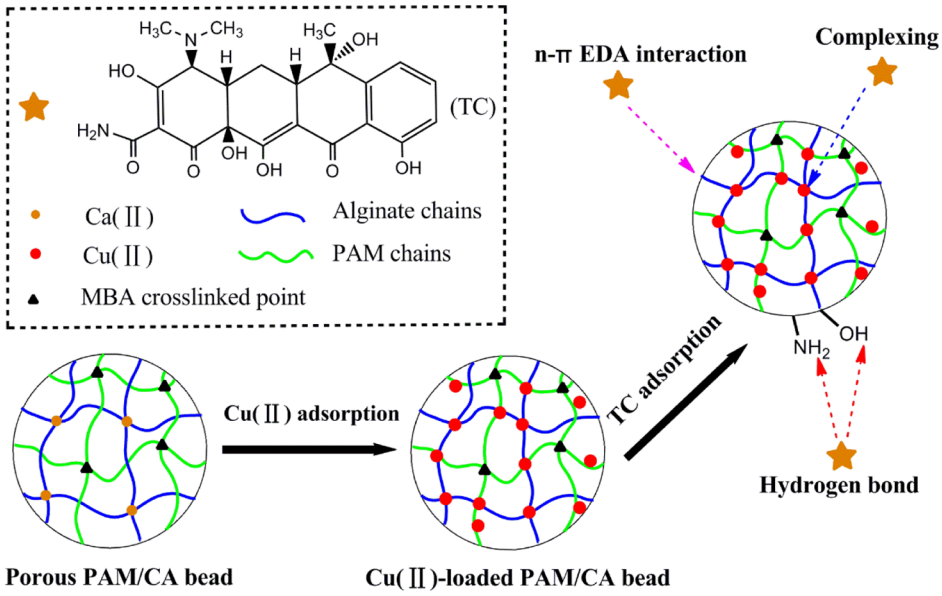

Figure 10. Possible chemisorption mechanism of TC onto the adsorbent.

O−H/C−O−C were shifted to the lower binding energies of 531.40, 532.48, and 533.26 eV, respectively, indicating the increment in the density of electron clouds around these active functional groups. These results demonstrated that the corresponding active oxygen-containing functional groups (hydroxyl and carbonyl groups in the beads) might participate in the adsorption of TC through the strong n−π electron donor−acceptor (n−π EDA) interaction and hydrogen bonding due to the existence of the benzene rings and highly electronegative atoms in the TC molecule.[21] In addition, the Cu 2p high-resolution spectra of PAM/CA@Cu after TC adsorption are presented in Figure S5d. The characteristic peak positions of Cu(II) $2p_{1/2}$, Cu(I) $2p_{1/2}$, Cu(II) $2p_{3/2}$, and Cu(I) $2p_{3/2}$ were shifted to 954.11, 952.15, 934.45, and 932.8 eV, respectively. These alterations in the binding energies before and after TC adsorption might be due to the specific interaction between Cu and the oxygen or nitrogen of the TC molecule, indicating that the hydroxyl, carbonyl, and amino groups of the TC molecule donated a large amount of electrons to Cu to form a complex of TC−Cu through the cation bonding bridge.[21,22] The inferred chemisorption mechanism of TC onto PAM/CA@Cu was illustrated in Figure 10. Based on the above analysis, it was deduced that the main mechanisms of TC adsorption on PAM/CA@Cu should be controlled by physisorption (electrostatic interaction and hydrophobic interaction) and chemisorption (n−π EDA interaction, hydrogen bonding, and complexing).

3. CONCLUSIONS

In summary, we attempt to propose a cost-efficient and effective method to reuse the porous PAM/CA beads after the removal of Cu(II) ions for adsorption of TC from aqueous solutions. The porous PAM/CA exhibited good adsorption capacity toward Cu(II) ions under batch and column modes. The porous PAM/CA after the removal of Cu(II) ions (PAM/CA@Cu) were stable enough and could be suitable for TC adsorption at a pH > 4.0, showing very little leakage of Cu(II) ions. The optimum adsorption capacity of TC was observed at around pH 5.0. The PAM/CA@Cu achieved a maximum TC adsorption capacity of 356.57 mg/g predicted by the Langmuir model at pH 5.0 and 30 °C, which was higher than most of the reported adsorbents. The regenerated PAM/CA@Cu obtained a decrease of 7% in the adsorption capacity for TC removal after three cycles. Results revealed that physisorption (electrostatic interaction and hydrophobic interaction) and chemisorption (n−π EDA interaction, hydrogen bonding, and complexing) corporately controlled the adsorption of TC onto PAM/CA@Cu. Overall, the PAM/CA@Cu could be utilized as an efficient biosorbent for adsorption of TC, which seems to achieve the purpose of treating waste with waste.

4. MATERIALS AND EXPERIMENTAL SECTION

4.1. Materials. SA, acrylamide (AM, 99%), PEG (M_n = 400 g/mol, 98%), *N*,*N*,*N*′,*N*′-tetramethylethylenediamine (TEMED, 99%), *N*,*N*′-MBA (99%), and TC were purchased from Aladdin (Shanghai, China). Calcium chloride dihydrate ($CaCl_2{\cdot}2H_2O$), ammonium persulfate (APS), copper nitrate trihydrate ($Cu(NO_3)_2{\cdot}3H_2O$), hydrochloric acid (HCl), and sodium hydroxide (NaOH) were obtained from Shanghai Experiment Reagent Co. (Shanghai, China). All chemicals and reagents were of the analytical grade or higher and directly used without any purification. Deionized (DI) water (18 MΩ cm, TST-P, Shijiazhuang, China) was used for all experiments.

4.2. Preparation of Porous PAM/CA. In brief, 1.00 g of SA was dissolved in 50 mL of DI water under continuous magnetic stirring overnight to obtain a homogeneous mixture at room temperature. Then, 3.84 g of AM, MBA (5 mol % AM), TEMED (0.5 mL), and PEG with a certain molar ratio of PEG/monomers (SA and AM) (=1:2) were added into the above mixture. The mixture was bubbled with nitrogen for 30 min and allowed to stand for at least 30 min before use. The obtained homogeneous collosol was subsequently transferred to a constant pressure funnel and dropped into a preformulated solution of 3% (w/v) $CaCl_2$ and 0.5% (w/v) APS through a 200-μL pipette tip (Huabo Experimental Equipment Co., Haimen, China), which was also previously nitrogen-purged for 30 min. Spherical and uniform beads were obtained and kept for 24 h in the solution under a nitrogen atmosphere with continuous magnetic stirring to warrant the adequate cross-linking. The gelated beads were washed with

https://dx.doi.org/10.1021/acsomega.0c05807
ACS Omega 2021, 6, 6240−6251

DI water every 6 h for at least 72 h to wash out PEG and unreacted materials. Finally, the obtained porous PAM/CA beads were freeze-dried and stored at room temperature in a desiccator over silica gel before use, and they can maintain chemical stability with time. Similar storage conditions can be seen in the previous study.[51]

4.3. Batch Adsorption of Cu(II) Ions by Porous PAM/CA Beads. Batch adsorption experiments of Cu(II) ions were investigated by immersing freeze-dried samples (0.05 g) in the 50 mL of Cu(II) solution from its nitrate salt (the initial concentration of Cu(II) ions was 100 mg/L), which was shaken in an air bath thermostatic oscillator (THZ-82A, Kexing, China) at 160 rpm and 303 K for 24 h. The concentrations of Cu(II) ions in the solutions were measured by a flame atomic absorption spectrometer (AA-6800F, Shimadzu Co., Japan). The adsorption capacity of Cu(II) ions was calculated by the following equation

$$q_t = \frac{(C_o - C_t) \times V}{m} \quad (1)$$

where q_t is the amount of Cu(II) ions adsorbed on unit mass of the beads (mg/g); C_o and C_t are the concentrations of Cu(II) ions in the aqueous solution before and after adsorption for t (min) (mg/L), respectively; V is the volume of the aqueous solution (L); m is the weight of freeze-dried beads (g).

The effect of solution pH was investigated by varying the initial pH of Cu(II) solution from 2.0 to 6.0 using a 0.1 mol/L HCl or NaOH solution. The adsorption kinetics was conducted at around pH 5.0 and 30 °C, and the mixture was taken out for Cu(II) concentration analysis periodically at different time intervals. The same analytical method as mentioned above was employed to detect the adsorption capacity. The obtained kinetics data were regressed by the nonlinear pseudo-first-order and pseudo-second-order models, as described in the Supporting Information. In the isotherm experiments, the initial Cu(II) concentration was controlled in the range from 25 to 400 mg/L, and all experiments were conducted at 30 °C and around pH 5.0. The isotherm data were further analyzed using Langmuir and Freundlich models given in the Supporting Information. All experiments were conducted in triplicate.

4.4. Adsorption Stability of Cu(II) Ions onto Porous PAM/CA Beads. To evaluate the stability of Cu(II) ions onto porous PAM/CA beads, the desorption behavior of Cu(II) ions from PAM/CA@Cu was investigated in solutions under different pH conditions. When the adsorption process was completed, 0.025 g of PAM/CA@Cu was added to nine centrifuge tubes with 25 mL of DI water. The solution pH of each tube was adjusted to 0.7, 2.0, 3.0, 4.0, 5.0, 6.0, 7.0, 9.0, and 11.0, respectively. After being shaken at 303 K for 24 h, the solutions were filtered and analyzed for the desorbed Cu(II) ions. The desorption percentage was examined by the ratio of Cu(II) ions in the elution medium to the equilibrium adsorption capacity.

4.5. Desorption and Reusability of Porous PAM/CA Beads. For cyclic desorption and regeneration tests, 0.05 g of porous PAM/CA beads were added into 50 mL of Cu(II) solution (100 mg/L) for 12 h under the same procedure as adsorption experiments. The porous PAM/CA-Cu was then regenerated in 50 mL of HCl solution (0.2 mol/L) for 2 h and then reused after repeated washing by DI water until the pH was neutral for the next adsorption tests. These steps together were called one cycle. Five cycles were conducted to investigate the reusability and stability of the adsorbent.

4.6. Column Adsorption of Cu(II) Ions by Porous PAM/CA Beads. A fixed-bed column with 1.5 cm inner diameter and 30 cm height was employed in column-mode studies to evaluate the potential of the obtained beads for practical applications. The adsorption of Cu(II) ions was carried out for two water samples containing Cu(II) ions. The first sample was real electroplating wastewater collected from nearby an electroplating factory in Guangdong Province. Based on the chemical analysis, the main composition of the sewage was determined as follows: pH 2.2, electrical conductivity 2.73 mS/cm, chemical oxygen demand 22.7 mg/L, Cl^- 15.49 mg/L, SO_4^{2-} 851.75 mg/L, Na^+ 10.42 mg/L, K^+ 3.41 mg/L, Zn^{2+} 0.40 mg/L and Cu^{2+} 304.4 mg/L. The real electroplating wastewater sample was used for column test without any pH alterations. The second sample was a synthetic solution, which was spiked with $Cu(NO_3)_2$ to get a final solution containing 304.4 mg/L of Cu(II) ions, and the solution pH was adjusted to 2.2. The two water samples were pumped upward and passed through the packed bed of freeze-dried adsorbents (2 g, 18 cm bed height) with a specific influent flow rate of 2 mL/min. The effluent samples were collected at regular time intervals for the residual Cu(II) concentration. Column adsorption experiments were examined at 30 °C and continued until exhaustion point (C_t/C_o = 90%) achieved.[11] The total amount of adsorbed Cu(II) ions (q_{total}, mg) and the equilibrium adsorption capacity of Cu(II) ions (q_e, mg/g) in the column were determined by the following eqs 2 and 3.[52,53]

$$q_{total} = \frac{Q}{1000}\int_{t=0}^{t=T_{total}} (C_o - C_t)dt \quad (2)$$

$$q_e = \frac{q_{total}}{m} \quad (3)$$

where Q (mL/min) represents the volumetric flow rate, T_{total} (min) is the horizontal time of exhaustion point, m (g) presents the mass of adsorbent, C_o (mg/L) and C_t (mg/L) are the influent Cu(II) concentration and effluent Cu(II) concentration at specific intervals, respectively.

4.7. Removal of TC by PAM/CA@Cu. Porous PAM/CA beads were added to $Cu(NO_3)_2$ aqueous solution (the initial concentration of Cu(II) ions was 100 mg/L) under continuous stirring at room temperature for 24 h to prepare the PAM/CA@Cu beads. In the $Cu(NO_3)_2$ solution, no precipitation of $Cu(OH)_2$ was observed to interfere during the adsorption process. Finally, the PAM/CA@Cu beads were washed with DI water, freeze-dried, and utilized as an adsorbent for the removal of TC. The adsorption experiments of TC were carried out in batch mode. The TC concentration in solution was measured by UV spectrophotometry at 360 nm.[32] PAM/CA@Cu beads (0.025 g) were added into a solution of TC (25 mL, 50 mg/L) and shaken at 160 rpm and 30 °C for 24 h. The pH effect on TC adsorption was investigated by adjusting the solution pH in the range from 2.0 to 10.0 using 0.1 mol/L HCl/NaOH solution. The effect of initial TC concentration was carried out by varying the initial TC concentration from 1 to 500 mg/L at pH 5.0. The effect of ionic strength on TC adsorption was performed by picking a NaCl solution of 0−0.1 mol/L. Besides, the effect of other coexisting salts was also carried out by adding other salts (KCl, $NaNO_3$, Na_2SO_4, $MgCl_2$, and $CaCl_2$, respectively) with the concentration of 0.1 mol/L into the solution. The adsorption kinetics of TC was

https://dx.doi.org/10.1021/acsomega.0c05807
ACS Omega 2021, 6, 6240−6251

carried out by measuring the adsorption capacity of TC as a function of contact time (0−720 min) at pH around 5.0. Other experimental parameters were described at the start of this section. The adsorption isotherms were carried out by subjecting 0.025 g of PAM/CA@Cu into 25 mL of TC solution whose concentration varied in the range of 25−500 mg/L at pH around 5.0, and the contact time was 24 h to ensure an equilibrium adsorption. The analytical methods about the adsorption data could be seen in the Supporting Information.

4.8. Reusability Study of PAM/CA@Cu. The cyclic adsorption and desorption experiments were repeated to investigate the potential application of PAM/CA@Cu for TC removal. PAM/CA@Cu beads (0.025 g) were added to 25 mL of TC solution (50 mg/L) for 12 h under the same procedure as mentioned above. After equilibrium adsorption, the beads were placed into 25 mL of NaOH solution (0.2 mol/L) for 12 h to achieve desorption. Then, they were washed with DI water and immersed in 100 mg/L Cu(II) solution undergoing activation for 12 h. Finally, the regenerated beads were obtained and reused for the next adsorption experiments. The adsorption−desorption experiments were conducted for three cycles.

4.9. Material Characterization. The morphological structures of samples were observed by a scanning electron microscope (JSM-7001F, JEOL, Japan). The chemical structures of samples were analyzed by FTIR spectroscopy (Tensor 27, Bruker, Germany). The specific surface area and porosity of samples were measured by common nitrogen adsorption−desorption isotherms using a surface area and porosity analyzer (ASAP2460 Version 3.00, Micromeritics). The surface area of samples was calculated according to the BET method, and the pore size distribution curve was obtained from the desorption branch calculated by the BJH method.[54] XPS (250XI, Thermo ESCALAB) analyses of samples before and after adsorption were carried out by using an Al Kα ($h\nu$ = 1486.6 eV, 150 W) X-ray radiation with a pass energy of 30 eV, and all the binding energies were calibrated against the C 1s peak at 284.8 eV.[22,55] The point of zero charge (pH_{pzc}) for samples was determined by measuring initial pH (pH_i) and final pH (pH_f) of the solution. The value of pH_{pzc} is the point where the curve of ΔpH (=$pH_f - pH_i$) versus pH_i crosses the line equal to zero by the pH drift method.[12,56,57]

■ ASSOCIATED CONTENT

Supporting Information

The Supporting Information is available free of charge at https://pubs.acs.org/doi/10.1021/acsomega.0c05807.

> Adsorption kinetics model and fitting, adsorption isotherms model and fitting, point of zero charge (pH_{pzc}) for PAM/CA@Cu, effect of coexisting salts on TC removal, SEM images of the samples, textural characteristics of the samples, and XPS spectra of C 1s and Cu 2p peaks for the samples (PDF)

■ AUTHOR INFORMATION

Corresponding Authors

Huayong Luo − *School of Civil Engineering, Guangzhou University, Guangzhou 510006, China*; orcid.org/0000-0001-8972-597X; Email: lhy0909@gzhu.edu.cn

Hongwei Rong − *School of Civil Engineering, Guangzhou University, Guangzhou 510006, China*; Email: gzdxrhw@163.com

Authors

Yu Liu − *School of Civil Engineering, Guangzhou University, Guangzhou 510006, China*

Hanxing Lu − *School of Civil Engineering, Guangzhou University, Guangzhou 510006, China*

Qian Fang − *School of Civil Engineering, Guangzhou University, Guangzhou 510006, China*

Complete contact information is available at: https://pubs.acs.org/10.1021/acsomega.0c05807

Author Contributions

Huayong Luo leads the research. All authors have given approval to the final version of the manuscript.

Notes

The authors declare no competing financial interest.

■ ACKNOWLEDGMENTS

We would like to thank the Natural Science Foundation of Guangdong Province (2020A1515010856), the National Natural Science Foundation of China (51608133 and 51778155), and the Guangzhou University's training program for excellent new-recruited doctors (YB201718) for the financial support. We also thank the Analytical and Testing Center of Guangzhou University for related analysis.

■ REFERENCES

(1) Jiang, H.; Yang, Y.; Lin, Z.; Zhao, B.; Wang, J.; Xie, J.; Zhang, A. Preparation of a novel bio-adsorbent of sodium alginate grafted polyacrylamide/graphene oxide hydrogel for the adsorption of heavy metal ion. *Sci. Total Environ.* **2020**, *744*, 140653.

(2) Kong, A.; He, B.; Liu, G.; Lu, X.; Hao, Y.; Bao, X.; Yan, F.; Li, J. A Novel green biosorbent from chitosan modified by sodium phytate for copper (II) ion removal. *Polym. Adv. Technol.* **2018**, *29*, 285−293.

(3) Kong, A.; Ji, Y.; Ma, H.; Song, Y.; He, B.; Li, J. A novel route for the removal of Cu(II) and Ni(II) ions via homogeneous adsorption by chitosan solution. *J. Cleaner Prod.* **2018**, *192*, 801−808.

(4) Bădescu, I. S.; Bulgariu, D.; Ahmad, I.; Bulgariu, L. Valorisation possibilities of exhausted biosorbents loaded with metal ions−a review. *J. Environ. Manage.* **2018**, *224*, 288−297.

(5) Lucaci, A. R.; Bulgariu, D.; Popescu, M.-C.; Bulgariu, L. Adsorption of Cu(II) Ions on Adsorbent Materials Obtained from Marine Red Algae Callithamnion corymbosum sp. *Water* **2020**, *12*, 372.

(6) Karami, S.; Zeynizadeh, B. Reduction of 4-nitrophenol by a disused adsorbent: EDA-functionalized magnetic cellulose nanocomposite after the removal of Cu^{2+}. *Carbohydr. Polym.* **2019**, *211*, 298−307.

(7) Wu, J.; Cheng, X.; Li, Y.; Yang, G. Constructing biodegradable nanochitin-contained chitosan hydrogel beads for fast and efficient removal of Cu(II) from aqueous solution. *Carbohydr. Polym.* **2019**, *211*, 152−160.

(8) Ma, J.; Ma, Y.; Yu, F.; Dai, X. Rotating magnetic field-assisted adsorption mechanism of pollutants on mechanically strong sodium alginate/graphene/L-cysteine beads in batch and fixed-bed column systems. *Environ. Sci. Technol.* **2018**, *52*, 13925−13934.

(9) Zhang, W.; Deng, Q.; He, Q.; Song, J.; Zhang, S.; Wang, H.; Zhou, J.; Zhang, H. A facile synthesis of core-shell/bead-like poly (vinyl alcohol)/alginate@PAM with good adsorption capacity, high adaptability and stability towards Cu(II) removal. *Chem. Eng. J.* **2018**, *351*, 462−472.

(10) Lucaci, A. R.; Bulgariu, D.; Ahmad, I.; Bulgariu, L. Equilibrium and kinetics studies of metal ions biosorption on alginate extracted

from marine red algae biomass (callithamnion corymbosum sp.). *Polymers* **2020**, *12*, 1888.
(11) Luo, H.; Zeng, X.; Liao, P.; Rong, H.; Zhang, T. C.; Jason Zhang, Z.; Meng, X. Phosphorus removal and recovery from water with macroporous bead adsorbent constituted of alginate-Zr^{4+} and PNIPAM-interpenetrated networks. *Int. J. Biol. Macromol.* **2019**, *126*, 1133−1144.
(12) Luo, H.; Rong, H.; Zhang, T. C.; Zeng, X.; Wan, J. Amino-functionalized magnetic zirconium alginate beads for phosphate removal and recovery from aqueous solutions. *J. Appl. Polym. Sci.* **2019**, *136*, 46897.
(13) Dragan, E. S. Design and applications of interpenetrating polymer network hydrogels. A review. *Chem. Eng. J.* **2014**, *243*, 572−590.
(14) Dai, J.; Yang, H.; Yan, H.; Shangguan, Y.; Zheng, Q.; Cheng, R. Phosphate adsorption from aqueous solutions by disused adsorbents: Chitosan hydrogel beads after the removal of copper(II). *Chem. Eng. J.* **2011**, *166*, 970−977.
(15) Singh, T.; Singhal, R. Reuse of a waste adsorbent poly(AAc/AM/SH)-Cu superabsorbent hydrogel, for the potential phosphate ion removal from waste water: Matrix effects, adsorption kinetics, and thermodynamic studies. *J. Appl. Polym. Sci.* **2013**, *129*, 3126−3139.
(16) Ehtesabi, H.; Roshani, S.; Bagheri, Z.; Yaghoubi-Avini, M. Carbon dots—Sodium alginate hydrogel: A novel tetracycline fluorescent sensor and adsorber. *J. Environ. Chem. Eng.* **2019**, *7*, 103419.
(17) Zhu, H.; Chen, T.; Liu, J.; Li, D. Adsorption of tetracycline antibiotics from an aqueous solution onto graphene oxide/calcium alginate composite fibers. *RSC Adv.* **2018**, *8*, 2616−2621.
(18) Jin, J.; Yang, Z.; Xiong, W.; Zhou, Y.; Xu, R.; Zhang, Y.; Cao, J.; Li, X.; Zhou, C. Cu and Co nanoparticles co-doped MIL-101 as a novel adsorbent for efficient removal of tetracycline from aqueous solutions. *Sci. Total Environ.* **2019**, *650*, 408−418.
(19) Ravikumar, K. V. G.; Kubendiran, H.; Ramesh, K.; Rani, S.; Mandal, T. K.; Pulimi, M.; Natarajan, C.; Mukherjee, A. Batch and column study on tetracycline removal using green synthesized NiFe nanoparticles immobilized alginate beads. *Environ. Technol. Innovation* **2020**, *17*, 100520.
(20) Huang, B.; Liu, Y.; Li, B.; Liu, S.; Zeng, G.; Zeng, Z.; Wang, X.; Ning, Q.; Zheng, B.; Yang, C. Effect of Cu(II) ions on the enhancement of tetracycline adsorption by Fe_3O_4@SiO_2-Chitosan/graphene oxide nanocomposite. *Carbohydr. Polym.* **2017**, *157*, 576−585.
(21) Zhang, X.; Lin, X.; He, Y.; Chen, Y.; Luo, X.; Shang, R. Study on adsorption of tetracycline by Cu-immobilized alginate adsorbent from water environment. *Int. J. Biol. Macromol.* **2019**, *124*, 418−428.
(22) Zhang, X.; Lin, X.; He, Y.; Luo, X. Phenolic hydroxyl derived copper alginate microspheres as superior adsorbent for effective adsorption of tetracycline. *Int. J. Biol. Macromol.* **2019**, *136*, 445−459.
(23) Nasrollahzadeh, M.; Sajjadi, M.; Iravani, S.; Varma, R. S. Starch, cellulose, pectin, gum, alginate, chitin and chitosan derived (nano)-materials for sustainable water treatment: A review. *Carbohydr. Polym.* **2021**, *251*, 116986.
(24) Zhu, H.; Fu, Y.; Jiang, R.; Yao, J.; Xiao, L.; Zeng, G. Optimization of copper(II) adsorption onto novel magnetic calcium alginate/maghemite hydrogel beads using response surface methodology. *Ind. Eng. Chem. Res.* **2014**, *53*, 4059−4066.
(25) Vakili, M.; Deng, S.; Liu, D.; Li, T.; Yu, G. Preparation of aminated cross-linked chitosan beads for efficient adsorption of hexavalent chromium. *Int. J. Biol. Macromol.* **2019**, *139*, 352−360.
(26) Huang, G.; Wang, D.; Ma, S.; Chen, J.; Jiang, L.; Wang, P. A new, low-cost adsorbent: preparation, characterization, and adsorption behavior of Pb(II) and Cu(II). *J. Colloid Interface Sci.* **2015**, *445*, 294−302.
(27) Fan, C.; Li, K.; Li, J.; Ying, D.; Wang, Y.; Jia, J. Comparative and competitive adsorption of Pb(II) and Cu(II) using tetraethylenepentamine modified chitosan/$CoFe_2O_4$ particles. *J. Hazard. Mater.* **2017**, *326*, 211−220.
(28) Dai, J.; Meng, X.; Zhang, Y.; Huang, Y. Effects of modification and magnetization of rice straw derived biochar on adsorption of tetracycline from water. *Bioresour. Technol.* **2020**, *311*, 123455.
(29) Liang, J.; Fang, Y.; Luo, Y.; Zeng, G.; Deng, J.; Tan, X.; Tang, N.; Li, X.; He, X.; Feng, C.; Ye, S. Magnetic nanoferromanganese oxides modified biochar derived from pine sawdust for adsorption of tetracycline hydrochloride. *Environ. Sci. Pollut. Res.* **2019**, *26*, 5892−5903.
(30) Jin, L.; Amaya-Mazo, X.; Apel, M. E.; Sankisa, S. S.; Johnson, E.; Zbyszynska, M. A.; Han, A. Ca^{2+} and Mg^{2+} bind tetracycline with distinct stoichiometries and linked deprotonation. *Biophys. Chem.* **2007**, *128*, 185−196.
(31) He, J.; Ni, F.; Cui, A.; Chen, X.; Deng, S.; Shen, F.; Huang, C.; Yang, G.; Song, C.; Zhang, J.; Tian, D.; Long, L.; Zhu, Y.; Luo, L. New insight into adsorption and co-adsorption of arsenic and tetracycline using a Y-immobilized graphene oxide-alginate hydrogel: Adsorption behaviours and mechanisms. *Sci. Total Environ.* **2020**, *701*, 134363.
(32) Zhuang, Y.; Yu, F.; Ma, J.; Chen, J. Enhanced adsorption removal of antibiotics from aqueous solutions by modified alginate/graphene double network porous hydrogel. *J. Colloid Interface Sci.* **2017**, *507*, 250−259.
(33) Zhuang, Y.; Kong, Y.; Wang, X.; Shi, B. Novel one step preparation of a 3D alginate based MOF hydrogel for water treatment. *New J. Chem.* **2019**, *43*, 7202−7208.
(34) Ma, J.; Lei, Y.; Khan, M. A.; Wang, F.; Chu, Y.; Lei, W.; Xia, M.; Zhu, S. Adsorption properties, kinetics & thermodynamics of tetracycline on carboxymethyl-chitosan reformed montmorillonite. *Int. J. Biol. Macromol.* **2019**, *124*, 557−567.
(35) Nurhasanah, I.; Kadarisman; Gunawan, V.; Sutanto, H. Cerium oxide nanoparticles application for rapid adsorptive removal of tetracycline in water. *J. Environ. Chem. Eng.* **2020**, *8*, 103613.
(36) Ahamad, T.; Ruksana; Chaudhary, A. A.; Naushad, M.; Alshehri, S. M. Fabrication of $MnFe_2O_4$ nanoparticles embedded chitosan-diphenylureaformaldehyde resin for the removal of tetracycline from aqueous solution. *Int. J. Biol. Macromol.* **2019**, *134*, 180−188.
(37) Zhang, Z.; Lan, H.; Liu, H.; Qu, J. Removal of tetracycline antibiotics from aqueous solution by amino-Fe (III) functionalized SBA15. *Colloids Surf., A* **2015**, *471*, 133−138.
(38) Yang, Y.; Dong, R.; Zhu, Y.; Li, H.; Zhang, H.; Fan, X.; Chang, H. High-performance direct hydrogen peroxide fuel cells (DHPFCs) with silver nanowire-graphene hybrid aerogel as highly-conductive mesoporous electrodes. *Chem. Eng. J.* **2020**, *381*, 122749.
(39) Li, Y.; Liu, F.; Xia, B.; Du, Q.; Zhang, P.; Wang, D.; Wang, Z.; Xia, Y. Removal of copper from aqueous solution by carbon nanotube/calcium alginate composites. *J. Hazard. Mater.* **2010**, *177*, 876−880.
(40) Bakr, A.-S. A.; Moustafa, Y. M.; Khalil, M. M. H.; Yehia, M. M.; Motawea, E. A. Magnetic nanocomposite beads: synthesis and uptake of Cu(II) ions from aqueous solutions. *Can. J. Chem.* **2015**, *93*, 289−296.
(41) Fan, J.; Shi, Z.; Lian, M.; Li, H.; Yin, J. Mechanically strong graphene oxide/sodium alginate/polyacrylamide nanocomposite hydrogel with improved dye adsorption capacity. *J. Mater. Chem. A* **2013**, *1*, 7433−7443.
(42) Huang, Y.; Wu, H.; Shao, T.; Zhao, X.; Peng, H.; Gong, Y.; Wan, H. Enhanced copper adsorption by DTPA-chitosan/alginate composite beads: Mechanism and application in simulated electroplating wastewater. *Chem. Eng. J.* **2018**, *339*, 322−333.
(43) Zou, X.; Zhang, H.; Chen, T.; Li, H.; Meng, C.; Xia, Y.; Guo, J. Preparation and characterization of polyacrylamide/sodium alginate microspheres and its adsorption of MB dye. *Colloids Surf., A* **2019**, *567*, 184−192.
(44) Huang, Q.; Zhao, J.; Liu, M.; Chen, J.; Zhu, X.; Wu, T.; Tian, J.; Wen, Y.; Zhang, X.; Wei, Y. Preparation of polyethylene polyamine@tannic acid encapsulated MgAl-layered double hydroxide for the efficient removal of copper (II) ions from aqueous solution. *J. Taiwan Inst. Chem. Eng.* **2018**, *82*, 92−101.

https://dx.doi.org/10.1021/acsomega.0c05807
ACS Omega 2021, 6, 6240−6251

(45) Sutirman, Z. A.; Sanagi, M. M.; Abd Karim, K. J.; Wan Ibrahim, W. A.; Jume, B. H. Equilibrium, kinetic and mechanism studies of Cu(II) and Cd(II) ions adsorption by modified chitosan beads. *Int. J. Biol. Macromol.* **2018**, *116*, 255−263.
(46) Chen, B.; Zhao, H.; Chen, S.; Long, F.; Huang, B.; Yang, B.; Pan, X. A magnetically recyclable chitosan composite adsorbent functionalized with EDTA for simultaneous capture of anionic dye and heavy metals in complex wastewater. *Chem. Eng. J.* **2019**, *356*, 69−80.
(47) Lv, L.; Chen, N.; Feng, C.; Zhang, J.; Li, M. Heavy metal ions removal from aqueous solution by xanthate-modified cross-linked magnetic chitosan/poly(vinyl alcohol) particles. *RSC Adv.* **2017**, *7*, 27992−28000.
(48) Deng, J.; Liu, Y.; Liu, S.; Zeng, G.; Tan, X.; Huang, B.; Tang, X.; Wang, S.; Hua, Q.; Yan, Z. Competitive adsorption of Pb(II), Cd(II) and Cu(II) onto chitosan-pyromellitic dianhydride modified biochar. *J. Colloid Interface Sci.* **2017**, *506*, 355−364.
(49) Chao, S.; Li, X.; Li, Y.; Wang, Y.; Wang, C. Preparation of polydopamine-modified zeolitic imidazolate framework-8 functionalized electrospun fibers for efficient removal of tetracycline. *J. Colloid Interface Sci.* **2019**, *552*, 506−516.
(50) Yuan, Y.; Zhang, G.; Li, Y.; Zhang, G.; Zhang, F.; Fan, X. Poly(amidoamine) modified graphene oxide as an efficient adsorbent for heavy metal ions. *Polym. Chem.* **2013**, *4*, 2164−2167.
(51) Flamminii, F.; Di Mattia, C. D.; Nardella, M.; Chiarini, M.; Valbonetti, L.; Neri, L.; Difonzo, G.; Pittia, P. Structuring alginate beads with different biopolymers for the development of functional ingredients loaded with olive leaves phenolic extract. *Food Hydrocolloids* **2020**, *108*, 105849.
(52) Luo, H.; Rong, H.; Zeng, X.; Wang, R.; Chu, Z. Performance of phosphorus sorption on thermosensitive zirconium alginate hydrogel beads with full-interpenetrating network. *Chem. J. Chin. Univ.* **2018**, *39*, 2289−2297.
(53) Nguyen, T. A. H.; Ngo, H. H.; Guo, W. S.; Pham, T. Q.; Li, F. M.; Nguyen, T. V.; Bui, X. T. Adsorption of phosphate from aqueous solutions and sewage using zirconium loaded okara (ZLO): Fixed-bed column study. *Sci. Total Environ.* **2015**, *523*, 40−49.
(54) Chang, J. H.; Kim, J.; Lee, H. PNIPAm grafted amino-functionalized mesoporous silica for thermo-responsive chromium elimination. *Appl. Surf. Sci.* **2017**, *424*, 115−121.
(55) Chen, Z.; Luo, H.; Rong, H. Development of polyaminated chitosan-zirconium(IV) complex bead adsorbent for highly efficient removal and recovery of phosphorus in aqueous solutions. *Int. J. Biol. Macromol.* **2020**, *164*, 1183−1193.
(56) Liu, B.; Luo, H.; Rong, H.; Zeng, X.; Wu, K.; Chen, Z.; Lu, H.; Xu, D. Temperature-induced adsorption and desorption of phosphate on poly(acrylic acid-co-N-[3-(dimethylamino)propyl]acrylamide) hydrogels in aqueous solutions. *Desalin. Water Treat.* **2019**, *160*, 260−267.
(57) Jung, K.-W.; Jeong, T.-U.; Choi, J.-W.; Ahn, K.-H.; Lee, S.-H. Adsorption of phosphate from aqueous solution using electrochemically modified biochar calcium-alginate beads: Batch and fixed-bed column performance. *Bioresour. Technol.* **2017**, *244*, 23−32.

https://dx.doi.org/10.1021/acsomega.0c05807
ACS Omega 2021, 6, 6240−6251